Materials Today Energy 21 (2021) 100810

Contents lists available at ScienceDirect

Materials Today Energy

journal homepage: www.journals.elsevier.com/materials-today-energy/

Tuning power factors of two-dimensional Bi_2O_2Se nanoplates through vacancy engineering

Z. Wu [a], Y. Wang [a], G. Liu [a], X. Yang, T. Wei, H. Zhang, J. Zhou, J. Zhu*

National Laboratory of Solid State Microstructures, College of Engineering and Applied Sciences and Jiangsu Key Laboratory of Artificial Functional Materials, Nanjing University, Nanjing 210093, China

ARTICLE INFO

Article history:
Received 26 April 2021
Received in revised form
24 June 2021
Accepted 28 June 2021
Available online 6 July 2021

Keywords:
Thermoelectric
Band engineering
Self-doping
2D materials

ABSTRACT

Bi_2O_2Se, as a novel two-dimensional (2D) material, is attracting much attention owing to unique electrical and optoelectrical properties. Particularly, 2D Bi_2O_2Se with high mobility and a suitable bandgap has been predicted to be a promising thermoelectric material. Here, we performed systematic investigation of thermoelectric properties of 2D Bi_2O_2Se through both experimental measurements and theoretical calculations. It is found that the post-growth 2D Bi_2O_2Se nanoplates exhibit semi-metallic behavior because of existence of oxygen vacancies. Furthermore, vacancy engineering through annealing, which effectively tunes the concentration of oxygen vacancies, can significantly enhance the Seebeck coefficient of 2D Bi_2O_2Se (30–90 μV/K) and the power factor (1–2.7 μW/cm/K^2), competitive as an air-stable oxide thermoelectric material. Our results not only demonstrate the promising power factor of 2D Bi_2O_2Se, but also provide a general and alternative strategy of vacancy engineering for tuning the thermoelectric properties of low-dimensional materials.

1. Introduction

2D materials, in which electrons and phonons are restricted to a disparate 2D interlayer lattice, have been considered as promising thermoelectric materials due to their unique electronic and thermal properties. [1–4] Bi_2O_2Se, as an emerging 2D material, attracts much attention owing to intriguing electrical and optoelectronic properties [5–16]. For thermoelectric applications, bulk Bi_2O_2Se, with a similar structure as oxide thermoelectric materials [17,18] and low lattice thermal conductivity [19–22], has been studied extensively [23–25].

2D Bi_2O_2Se nanoplates are predicted to have a high power factor (PF) for thermoelectrics because of its ultrahigh mobility and appropriate bandgap [5,26,27]. Besides, it has been demonstrated in previous works that 2D Bi_2O_2Se nanoplate exhibits a low thermal conductivity (~1 W/m/K) due to low phonon group velocity and large Gruneisen parameters [21,22]. Gate-tunable high PF was observed in the planar grown Bi_2O_2Se nanoplate at low temperature (80–200 K), which was transferred by the polymethylmethacrylate (PMMA) method [28]. However, so far there have been no systematic studies of the thermoelectric properties of 2D Bi_2O_2Se. Also, thermoelectric properties in the high working temperature have not been investigated.

Here for the first time, we systematically investigate the thermoelectric properties of 2D Bi_2O_2Se through both calculation and experiment, and further tune the thermoelectric performance through oxygen vacancy engineering. The vertically grown 2D nanoplates inhibit the effect of polymer contamination. It is found that the thermoelectric properties of post-growth 2D Bi_2O_2Se nanoplates are dominated by oxygen vacancies, leading to semi-metallic behaviors. In addition, because of the high surface/volume ratio of 2D material, concentration of oxygen vacancies can be conveniently tuned through an annealing process under moderate conditions (Fig. 1a). As a result of this vacancy engineering, the band structures and carrier concentration can be modulated (Fig. 1b), which serves as a very effective knob to enhance the Seebeck coefficient and PF. Therefore, this work not only demonstrates the promising thermoelectric properties of 2D Bi_2O_2Se, but also provides a general and alternative strategy of vacancy engineering for low-dimensional materials.

2. Materials and methods

2.1. First-principles calculations

To resolve the band structures of Bi_2O_2Se with different O-vacancy concentrations (from 0 to 1/16), we performed the first-

* Corresponding author.
E-mail address: jiazhu@nju.edu.cn (J. Zhu).
[a] These authors contributed equally to this work.

https://doi.org/10.1016/j.mtener.2021.100810
2468-6069/

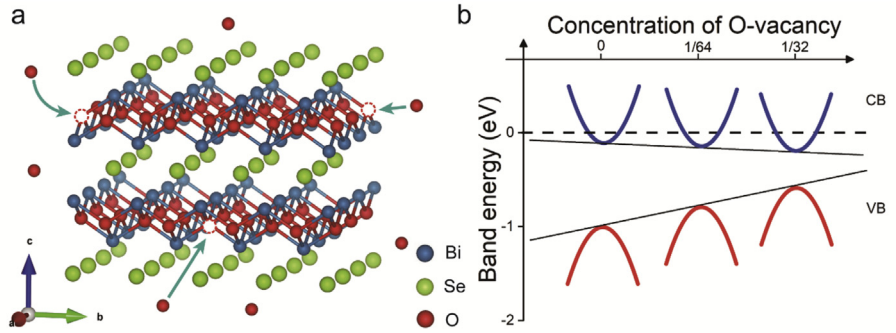

Fig. 1. Schematic of band modulation of 2D Bi_2O_2Se nanoplates through vacancy engineering. (a) Schematic of vacancy engineering of 2D Bi_2O_2Se nanoplates. The Bi, Se, and O atoms are shown in blue, green, and red colors, respectively. (b) Illustration of the strong dependence of band energy on the concentration of oxygen vacancy.

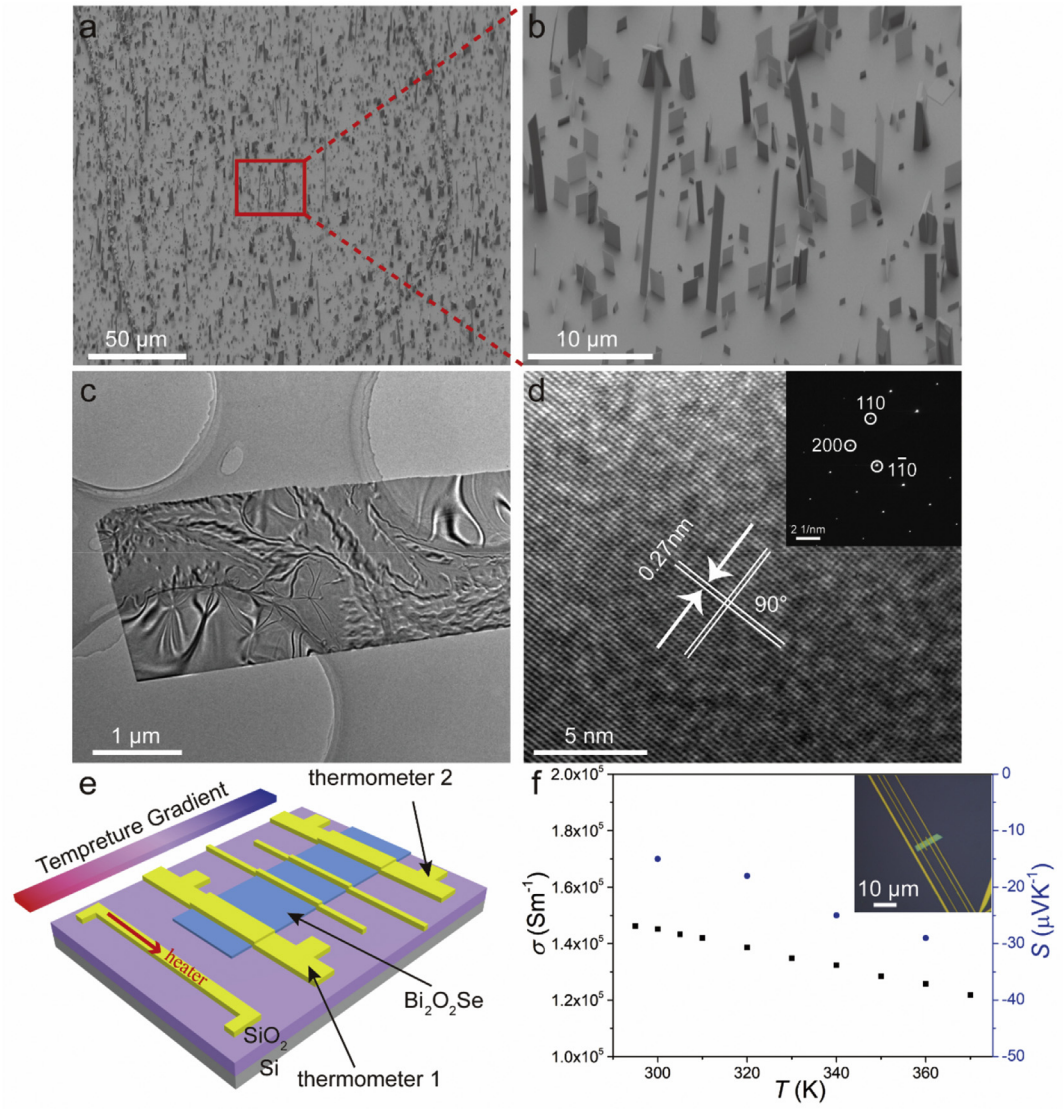

Fig. 2. Characterizations of Bi_2O_2Se nanoplates. (a) Large area SEM image of vertically grown 2D Bi_2O_2Se nanoplates. (b) Zoom-in SEM image of vertically grown 2D Bi_2O_2Se nanoplates. (c) TEM image of a Bi_2O_2Se nanoplate after transferred onto a holey carbon TEM grid. (d) High-resolution TEM image of Bi_2O_2Se nanoplate projected along the *c*-axis and inset shows an SAED pattern (inset). (e) Schematics for measuring Seebeck coefficient and electrical conductivity. (f) The dependence of Seebeck coefficient and conductivity on temperature (inset: the fabricated device).

principles calculations in the framework of density functional theory (DFT) with the program package CASTEP. The transport properties of Bi_2O_2Se before and after O_2 annealing were calculated by using semi-classical Boltzmann transport theory and the rigid band approach as implemented in the Boltzmann transport properties (BoltzTraP) program. The calculated carrier concentration, mobility, electrical conductivity and Seebeck coefficient as a function of temperature are shown in Figs. S5 and S6, respectively.

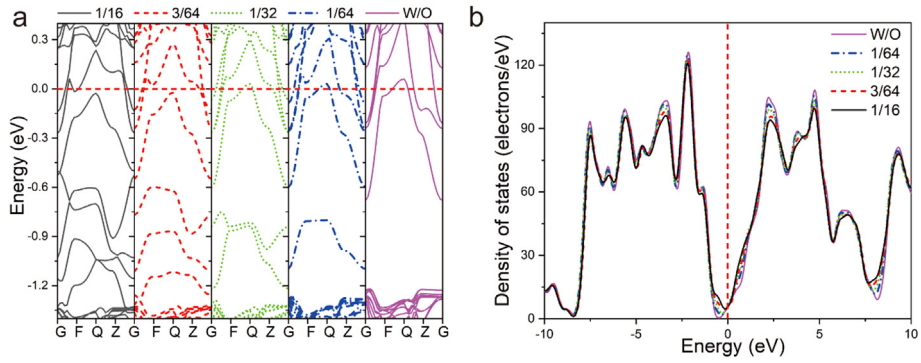

Fig. 3. Band structures and total density of states of Bi_2O_2Se with different oxygen vacancies. (a) Band structures of Bi_2O_2Se with different oxygen vacancies. (b) Total density of states (TDOS) of Bi_2O_2Se with different oxygen vacancies. The numbers 1/16, 3/64, 1/32, and 1/64 represent the concentration of oxygen vacancies relative to fully occupied Bi_2O_2Se. W/O represents the one without oxygen vacancy.

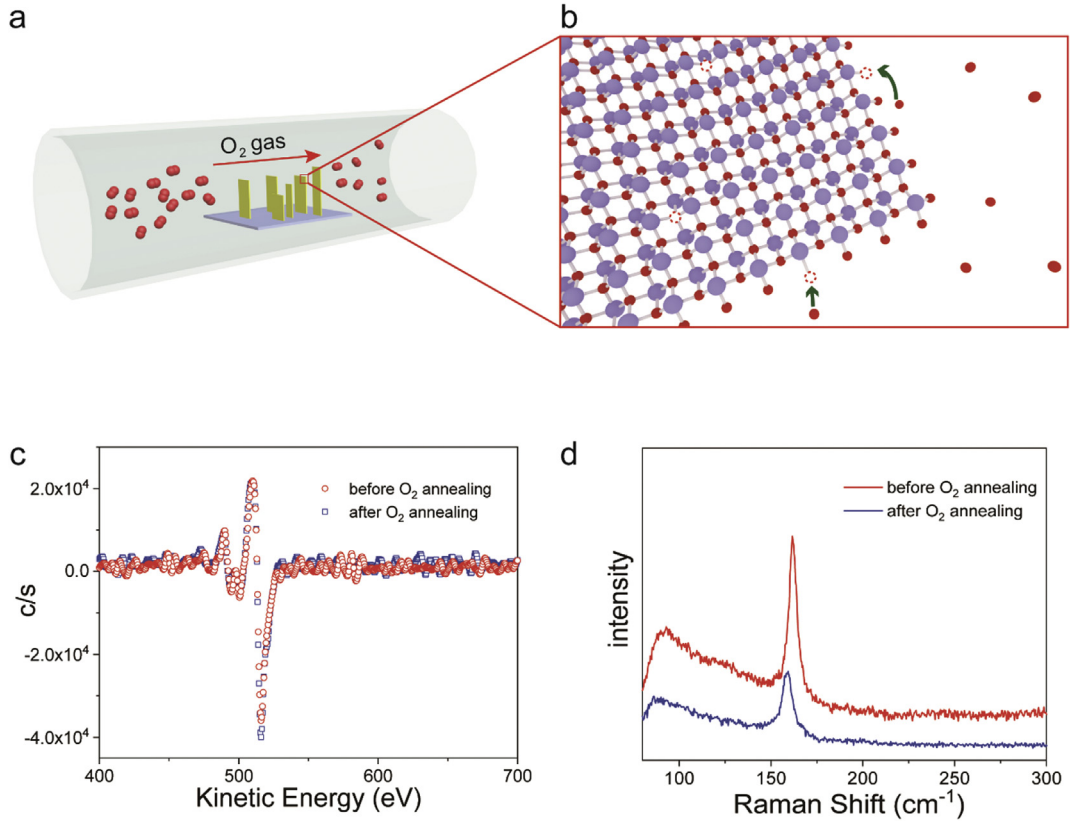

Fig. 4. Schematic of oxygen atoms filling vacancies and characterizations of Bi_2O_2Se nanoplates before and after O_2 annealing. (a) Schematic of vertically grown Bi_2O_2Se nanoplates annealing in O_2 atmosphere. (b) Schematic of oxygen atoms filling vacancies. (c) Auger electron spectra of comparison of changes in oxygen content before and after O_2 annealing. (d) Raman shift of 2D Bi_2O_2Se nanoplate before and after O_2 annealing.

2.2. Device fabrication

PMMA was spin-coated on a SiO_2/Si substrate carrying Bi_2O_2Se nanoplates. Electron beam lithography (EBL) was used to define the electrode patterns. With the predesigned pattern appeared, metal electrodes (Pd/Au, 10 nm/60 nm) were deposited by the electron beam evaporation (EBE) and PMMA was removed.

For characterizations of the Bi_2O_2Se nanoplates, optical microscope (Eclipse LV100D; Nikon), scanning electron microscope (SEM, Helios NanoLab 600i; FEI), transmission electron microscope (TEM, Tecnai F20; FEI), atomic force microscope (Cypher AFM; Oxford Instrument, Inc), Auger electron spectroscopy (AES, ULVAC-PHI 710), Hall effect system (LakeShore 8404), and Raman spectrum (Renishaw inVia Raman microscope) are performed.

3. Results and discussion

The Bi_2O_2Se nanoplates in this study are obtained through seed layer-assisted chemical vapor deposition (Fig. 2a). Those Bi_2O_2Se nanoplates are grown vertically on the substrates of cleaved fluorphlogopite mica (Fig. 2b), making them ideal for convenient and clean transfer, one of critical requirements for thermal measurements without contaminations or effects from substrates of growth. The TEM examination (Fig. 2c) reveals that those

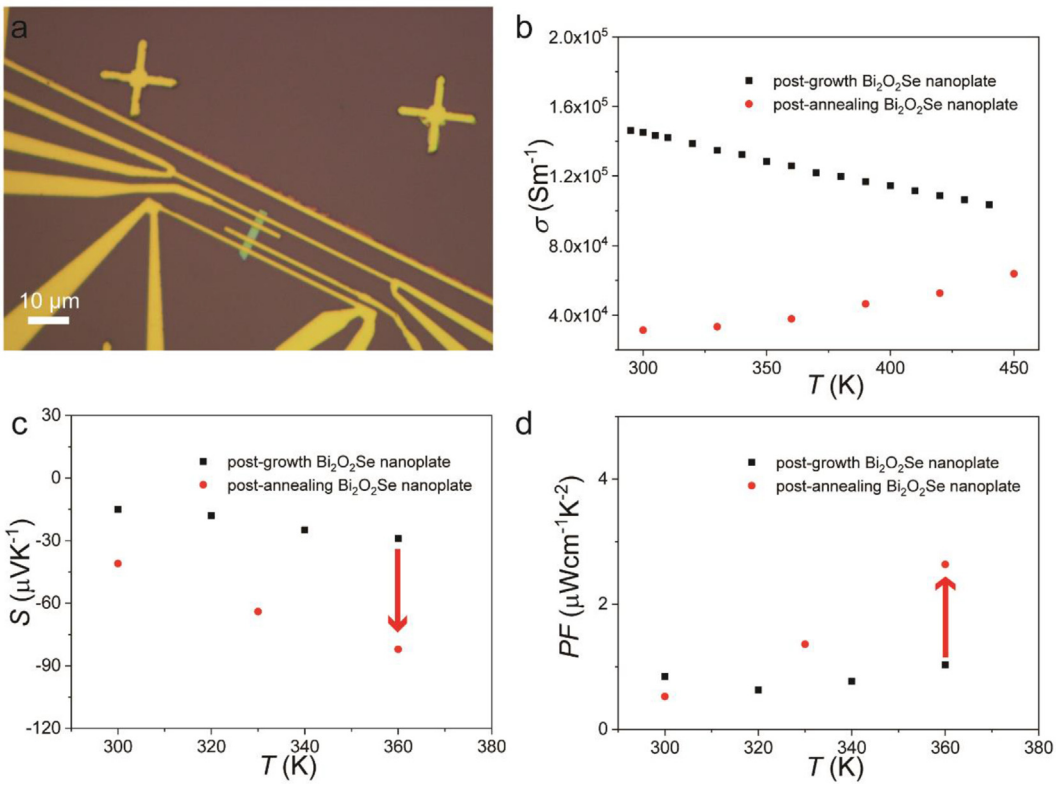

Fig. 5. Thermoelectric measurements of post-annealing Bi_2O_2Se nanoplates. (a) Micro-fabricated device of the Bi_2O_2Se nanoplates after treatment. (b, c, d) The dependence of measured conductivities, Seebeck coefficients, and PFs on the temperature of measurement.

nanoplates have a lattice spacing of 0.27 nm (Fig. 2d), consistent with the theoretical value of lattice constant of (110) Bi_2O_2Se [5–9]. The selected area diffraction (SAED) pattern (inset) confirms the high crystal quality with tetragonal structure of Bi_2O_2Se.

For the measurement of thermoelectric properties, Bi_2O_2Se nanoplates were transferred onto clean 285 nm SiO_2/Si substrates for EBL and EBE (Fig. 2e, details in Methods) [29]. The thickness of Bi_2O_2Se nanoplates was typically 13 nm, as determined by AFM (Fig. S1). It is found that the electrical conductivity of the Bi_2O_2Se nanoplate (inset of Fig. 2f) directly after growth approaches 1.5×10^5 S/m at room temperature. The electrical conductivity drops gradually as the temperature increases, exhibiting a semi-metallic behavior [30]. It does not correspond to the intrinsic semiconducting behavior of Bi_2O_2Se with a bandgap of 0.8 eV [5,7]. The highest Seebeck coefficient of these post-growth Bi_2O_2Se nanoplates is −30 μV/K, indicating the *n*-type behavior.

To reveal the fundamental mechanism governing the thermoelectric performances of these Bi_2O_2Se nanoplates, we performed theoretical calculations by DFT. It is found that O vacancies can shift the Fermi level deeply into conduction band, and consequentially lead to semi-metallic behavior. The density of states and band structures of different oxygen contents are shown in Fig. 3, in which the fraction represents the oxygen vacancy proportion. It is clear that there is no visible change in the total density of states near Fermi level with or without oxygen vacancy. However, as the concentration of oxygen vacancy increases, bandgap of Bi_2O_2Se nanoplate monotonically decreases (Fig. 3a). In addition, as the Fermi level shifts deeply into the conduction band, carrier concentration near Fermi level increases. Therefore, it is clear that significant amount of oxygen vacancies in the original post-growth Bi_2O_2Se nanoplate results in reduced band gap, increased carrier concentration, and decreased Seebeck coefficient. It also indicates that the modulation of oxygen vacancies will be the key to enhance Seebeck coefficient as well as the PF of these Bi_2O_2Se nanoplates.

Due to the large surface/volume ratio, it is more effective to achieve vacancy modulations for the Bi_2O_2Se nanoplates, compared to the bulk counterparts. Further calculation indicates that it is energetically more favorable for oxygen vacancies to exist on the surface of Bi_2O_2Se nanoplates rather than within the bulk (Table S1, Figs. S2 and S3). The dominant existence of oxygen vacancies on the surface, together with high surface/volume ratio of 2D nanoplates, offers unique advantage for vacancy engineering through annealing processes [13,31–33]. As illustrated in Fig. 4a, the mica substrate with vertically grown nanoplates is placed into the center of the quartz tube at 300°C for 2 h with 100 sccm oxygen gas. As oxygen gas molecules can conveniently reach the surface of these nanoplates, and it is energetically favorable for them to fill the oxygen vacancies (red dash circles), the oxygen vacancies can be reduced significantly through this process (Fig. 4b).

AES serves as a sensitive measurement to examine the changes in element content before and after annealing, as shown in Fig. 4c [34,35]. Quantitatively, it is found that annealing in O_2 atmosphere increases the content of oxygen by 6%. Raman spectrum (Fig. 4d) by a 632.8 nm laser indicates the characteristic A_{1g} peak position (~159 cm^{-1}) of the vertically grown sample, corresponding well with prior works [5–9]. After annealing in the O_2 atmosphere, the redshifted peak position indicates the decreased O-vacancy, which is consistent with the AES data.

As the decrease in O-vacancy can enlarge the bandgap and shift the Fermi level to the bottom of the conduction band, it is expected that vacancy engineering through annealing can enhance the Seebeck coefficient of *n*-type Bi_2O_2Se by tuning the carrier concentration ($S \sim (\pi/3n)^{2/3}$). The corresponding experiments and calculations of the carrier concentrations and mobilities of the

Bi_2O_2Se nanoplates are shown in Figs. S4 and S5. Consistent with our calculations, the Bi_2O_2Se nanoplates show decreased carrier concentration and increased mobility after annealing, indicating the reduction in oxygen defects.

To verify the effect of oxygen vacancy concentration on thermoelectric performance, we compared the thermoelectric properties of post-growth and post-annealing nanoplates (Fig. 5). Unlike the post-growth nanoplates' metallic behavior, the temperature dependence of conductivities of the post-annealing nanoplates (Fig. 5a) exhibits a semiconducting behavior (Fig. 5b), that the conductivity increases slowly with the rising temperature. The highest conductivity of nanoplates after annealing is 6.8×10^4 S/m at 450 K, which is reduced by 30% compared to that of post-growth nanoplates at the same temperature. The highest Seebeck coefficient of approximately −90 μV/K for the post-annealing nanoplate is more than a threefold enhancement compared to the post-growth ones at the same temperature (Fig. 5c). This experimental observation matches well with the calculated conductivity and Seebeck coefficient based on the oxygen vacancy concentration characterized by Auger electron spectra, as shown in Fig. S6.

The significant increase in Seebeck coefficient of post-annealing nanoplates, compared to the post-growth ones, also leads to enhanced PF. As shown in Fig. 5d, although the PFs of both post-growth and post-annealing nanoplates increase monotonically with the increasing temperatures, the PF of the nanoplate after annealing preserves a higher value over the entire temperature range. The highest value of PF reaches 2.7 $\mu W/cm/K^2$ at 360 K for nanoplates after annealing, which is closed to a threefold increase compared to the post-growth one, and comparable to the best value of doped bulk Bi_2O_2Se reported [24,25,36,37]. This effect of vacancy engineering is consistently observed in multiple nanoplates and experiments, as shown in Fig. S7. Considering that the thermal conductivity of the Bi_2O_2Se nanoplates is as low as 1 W/m/K at room temperature, the high PF demonstrated experimentally identifies the Bi_2O_2Se nanoplates as promising thermoelectric materials [21,22,38]. Through both calculations and experiments, it is confirmed that vacancy engineering by annealing can serve as an effective knob to tune the PFs of 2D Bi_2O_2Se nanoplates. Therefore, it provides an alternative and complementary strategy to improve the performance of low-dimensional thermoelectric materials.

4. Conclusion

For the first time, we systematically investigate the thermoelectric properties of the 2D Bi_2O_2Se nanoplates through both calculations and experiments. It is found that these nanoplates directly out of growth exhibit typical semi-metallic behavior, as a result of large amount of oxygen vacancies created during the growth. By taking advantage of high surface/volume ratio of these 2D nanoplates, the concentration of oxygen vacancies can be effectively tuned through an annealing process, which leads to significant increase in the Seebeck coefficient and PF. Therefore, these results not only demonstrate the promising thermoelectric properties of 2D Bi_2O_2Se, but also provide a general and alternative strategy of vacancy engineering for other low-dimensional materials.

Credit author statement

Jia Zhu and Zhen Wu designed and performed the experiments. Yuxi Wang performed the test of Seebeck coefficient and conductivity measurements. Guoliang Liu performed the theoretical calculations. Tianqi Wei and Jianfeng Zhou provided technical assistance. Xin Yang and Huizhen Zhang performed the sample transfer. Zhen Wu wrote the manuscript. Jia Zhu supervised the entire project.

Declaration of competing interest

The authors declare that they have no known competing financial interests or personal relationships that could have appeared to influence the work reported in this paper.

Acknowledgments

The authors acknowledge the micro-fabrication center of National Laboratory of Solid State Microstructures (NLSSM) for technique support. This work is supported by the National Natural Science Foundation of China (Nos. 21805132, 22005139, 51925204), Natural Science Foundation of Jiangsu Province (Nos. BK20180341), Program for Innovative Talents and Entrepreneur in Jiangsu and the Fundamental Research Funds for the Central Universities (Nos. 021314380135, 021314380128), and Excellent Research Program of Nanjing University (ZYJH005).

Appendix A. Supplementary data

Supplementary data to this article can be found online at https://doi.org/10.1016/j.mtener.2021.100810.

References

[1] J. Wu, Y. Chen, J. Wu, K. Hippalgaonkar, Perspectives on thermoelectricity in layered and 2D materials, Adv. Electron. Mater. 4 (2018) 1800248.
[2] M.S. Dresselhaus, G. Chen, M.Y. Tang, R.G. Yang, H. Lee, D.Z. Wang, Z.F. Ren, J.P. Fleurial, P. Gogna, New directions for low-dimensional thermoelectric materials, Adv. Mater. 19 (2007) 1043−1053.
[3] H.A. Eivari, Z. Sohbatzadeh, P. Mele, M.H.N. Assadi, Low thermal conductivity: fundamentals and theoretical aspects in thermoelectric applications, Mater. Tod. Energy 21 (2021) 100744.
[4] E. Liu, A. Negm, M.M.R. Howlader, Thermoelectric generation via tellurene for wearable applications: recent advances, research challenges, and future perspectives, Mater. Tod. Energy 20 (2021) 100625.
[5] J. Wu, H. Yuan, M. Meng, C. Chen, Y. Sun, Z. Chen, W. Dang, C. Tan, Y. Liu, J. Yin, Y. Zhou, S. Huang, H.Q. Xu, Y. Cui, H.Y. Hwang, Z. Liu, Y. Chen, B. Yan, H. Peng, High electron mobility and quantum oscillations in non-encapsulated ultrathin semiconducting Bi_2O_2Se, Nat. Nanotechnol. 12 (2017) 530−534.
[6] J. Wu, C. Tan, Z. Tan, Y. Liu, J. Yin, W. Dang, M. Wang, H. Peng, Controlled synthesis of high-mobility atomically thin bismuth oxyselenide crystals, Nano Lett. 17 (2017) 3021−3026.
[7] C. Chen, M. Wang, J. Wu, H. Fu, H. Yang, Z. Tian, T. Tu, H. Peng, Y. Sun, X. Xu, J. Jiang, N.B.M. Schröter, Y. Li, D. Pei, S. Liu, S.A. Ekahana, H. Yuan, J. Xue, G. Li, J. Jia, Z. Liu, B. Yan, H. Peng, Y. Chen, Electronic structures and unusually robust bandgap in an ultrahigh-mobility layered oxide semiconductor, Bi_2O_2Se, Sci. Adv. 4 (2018) eaat8355.
[8] Q. Fu, C. Zhu, X. Zhao, X. Wang, A. Chaturvedi, C. Zhu, X. Wang, Q. Zeng, J. Zhou, F. Liu, B.K. Tay, H. Zhang, S.J. Pennycook, Z. Liu, Ultrasensitive 2D Bi_2O_2Se phototransistors on silicon substrates, Adv. Mater. 31 (2019), e1804945.
[9] U. Khan, Y. Luo, L. Tang, C. Teng, J. Liu, B. Liu, H.M. Cheng, Controlled vapor-solid deposition of millimeter-size single crystal 2D Bi_2O_2Se for high-performance phototransistors, Adv. Funct. Mater. 29 (2019) 1807979.
[10] Z. Zhang, T. Li, Y. Wu, Y. Jia, C. Tan, X. Xu, G. Wang, J. Lv, W. Zhang, Y. He, J. Pei, C. Ma, G. Li, H. Xu, L. Shi, H. Peng, H. Li, Truly concomitant and independently expressed short- and long-term plasticity in a Bi_2O_2Se-based three-terminal memristor, Adv. Mater. 31 (2019), e1805769.
[11] J. Wu, Y. Liu, Z. Tan, C. Tan, J. Yin, T. Li, T. Tu, H. Peng, Chemical patterning of high-mobility semiconducting 2D Bi_2O_2Se crystals for integrated optoelectronic devices, Adv. Mater. 29 (2017) 1704060.
[12] J. Yin, Z. Tan, H. Hong, J. Wu, H. Yuan, Y. Liu, C. Chen, C. Tan, F. Yao, T. Li, Y. Chen, Z. Liu, K. Liu, H. Peng, Ultrafast and highly sensitive infrared photodetectors based on two-dimensional oxyselenide crystals, Nat. Commun. 9 (2018) 3311.
[13] J. Li, Z. Wang, Y. Wen, J. Chu, L. Yin, R. Cheng, L. Lei, P. He, C. Jiang, L. Feng, J. He, High-performance near-infrared photodetector based on ultrathin Bi_2O_2Se nanosheets, Adv. Funct. Mater. 28 (2018) 1706437.
[14] J. Wu, C. Qiu, H. Fu, S. Chen, C. Zhang, Z. Dou, C. Tan, T. Tu, T. Li, Y. Zhang, Z. Zhang, L.-M. Peng, P. Gao, B. Yan, H. Peng, Low residual carrier concentration and high mobility in 2D semiconducting Bi_2O_2Se, Nano Lett. 19 (2018) 197−202.

[15] Y. Liang, X. Zhou, W. Li, H. Peng, Preparation of two-dimensional [Bi_2O_2]-based layered materials: progress and prospects, Apl. Mater. 9 (2021), 060905.
[16] H. Tang, B. Shi, Y. Wang, C. Yang, S. Liu, Y. Li, R. Quhe, J. Lu, Layer-dependent photoabsorption and photovoltaic effects in two-dimensional Bi_2O_2X (X = S, Se, and Te), Phys. Rev. Appl. 15 (2021), 064037.
[17] Y. Liu, L.D. Zhao, Y. Liu, J. Lan, W. Xu, F. Li, B.P. Zhang, D. Berardan, N. Dragoe, Y.H. Lin, C.W. Nan, J.F. Li, H. Zhu, Remarkable enhancement in thermoelectric performance of BiCuSeO by Cu deficiencies, J. Am. Chem. Soc. 133 (2011) 20112−20115.
[18] L.-D. Zhao, J. He, D. Berardan, Y. Lin, J.-F. Li, C.-W. Nan, N. Dragoe, BiCuSeO oxyselenides: new promising thermoelectric materials, Energy Environ. Sci. 7 (2014) 2900−2924.
[19] X.L. Zhu, P.F. Liu, G. Xie, B.T. Wang, First-principles study of thermal transport properties in the two- and three-dimensional forms of Bi_2O_2Se, Phys. Chem. Chem. Phys. 21 (2019) 10931−10938.
[20] C. Wang, G. Ding, X. Wu, S. Wei, G. Gao, Electron and phonon transport properties of layered Bi2O2Se and Bi2O2Te from first-principles calculations, New J. Phys. 20 (2018) 123014.
[21] F. Yang, R. Wang, W. Zhao, J. Jiang, X. Wei, T. Zheng, Y. Yang, X. Wang, J. Lu, Z. Ni, Thermal transport and energy dissipation in two-dimensional Bi_2O_2Se, Appl. Phys. Lett. 115 (2019) 193103.
[22] Z. Wu, G. Liu, Y. Wang, X. Yang, T. Wei, Q. Wang, J. Liang, N. Xu, Z. Li, B. Zhu, H. Qi, Y. Deng, J. Zhu, Seed-induced vertical growth of 2D Bi_2O_2Se nanoplates by chemical vapor transport, Adv. Funct. Mater. 29 (2019) 1906639.
[23] B. Zhan, Y. Liu, X. Tan, J.L. Lan, Y.h. Lin, C.W. Nan, X.D. Zhou, Enhanced thermoelectric properties of Bi_2O_2Se ceramics by Bi deficiencies, J. Am. Ceram. Soc. 98 (2015) 2465−2469.
[24] R. Liu, J.-l. Lan, X. Tan, Y.-c. Liu, G.-k. Ren, C. Liu, Z.-f. Zhou, C.-w. Nan, Y.-h. Lin, Carrier concentration optimization for thermoelectric performance enhancement in n-type Bi_2O_2Se, J. Eur. Ceram. Soc. 38 (2018) 2742−2746.
[25] L. Pan, L. Zhao, X. Zhang, C. Chen, P. Yao, C. Jiang, X. Shen, Y. Lyu, C. Lu, L.D. Zhao, Y. Wang, Significant optimization of electron-phonon transport of n-type Bi_2O_2Se by mechanical manipulation of Se vacancies via shear exfoliation, ACS Appl. Mater. Interfaces 11 (2019) 21603−21609.
[26] J. Yu, Q. Sun, Bi_2O_2Se nanosheet: an excellent high-temperature n-type thermoelectric material, Appl. Phys. Lett. 112 (2018), 053901.
[27] J. Yu, T. Li, Q. Sun, Single-layer BiOBr: an effective p-type 2D thermoelectric material, J. Appl. Phys. 125 (2019) 205111.
[28] F. Yang, J. Wu, A. Suwardi, Y. Zhao, B. Liang, J. Jiang, J. Xu, D. Chi, K. Hippalgaonkar, J. Lu, Z. Ni, Gate-tunable polar optical phonon to piezoelectric scattering in few-layer Bi_2O_2Se for high-performance thermoelectrics, Adv. Mater. 33 (2021) 2004786.
[29] J. Kim, E. Fleming, Y. Zhou, L. Shi, Comparison of four-probe thermal and thermoelectric transport measurements of thin films and nanostructures with microfabricated electro-thermal transducers, J. Phys. D Appl. Phys. 51 (2018) 103002.
[30] L.-D. Zhao, G. Tan, S. Hao, J. He, Y. Pei, H. Chi, H. Wang, S. Gong, H. Xu, V.P. Dravid, C. Uher, G.J. Snyder, C. Wolverton, M.G. Kanatzidis, Ultrahigh power factor and thermoelectric performance in hole-doped single-crystal SnSe, Science 351 (2016) 141−144.
[31] S.M. Hus, A.-P. Li, Spatially-resolved studies on the role of defects and boundaries in electronic behavior of 2D materials, Prog. Surf. Sci. 92 (2017) 176−201.
[32] Z. Cai, B. Liu, X. Zou, H.M. Cheng, Chemical vapor deposition growth and applications of two-dimensional materials and their heterostructures, Chem. Rev. 118 (2018) 6091−6133.
[33] Z. Lin, B.R. Carvalho, E. Kahn, R. Lv, R. Rao, H. Terrones, M.A. Pimenta, M. Terrones, Defect engineering of two-dimensional transition metal dichalcogenides, 2D Mater. 3 (2016), 022002.
[34] N. Ott, Y. Yan, S. Ramamurthy, S. Kairy, N. Birbilis, Auger electron spectroscopy analysis of grain boundary microchemistry in an Al-Cu-Li alloy, Scripta Mater. 119 (2016) 17−20.
[35] T. Liu, X. Zhao, J. Li, Z. Liu, F. Liscio, S. Milita, B.C. Schroeder, O. Fenwick, Enhanced control of self-doping in halide perovskites for improved thermoelectric performance, Nat. Commun. 10 (2019) 5750.
[36] L. Pan, W.-D. Liu, J.-Y. Zhang, X.-L. Shi, H. Gao, Q.-f. Liu, X. Shen, C. Lu, Y.-F. Wang, Z.-G. Chen, Synergistic effect approaching record-high figure of merit in the shear exfoliated n-type $Bi_2O_{2-2x}Te_{2x}Se$, Nano Energy 69 (2020) 104394.
[37] X. Tan, J.L. Lan, K. Hu, B. Xu, Y. Liu, P. Zhang, X.Z. Cao, Y. Zhu, W. Xu, Y.H. Lin, C.W. Nan, Boosting the thermoelectric performance of Bi_2O_2Se by isovalent doping, J. Am. Ceram. Soc. 101 (2018) 4634−4644.
[38] Y. Sun, J. Zhang, S. Ye, J. Song, J. Qu, Progress report on property, preparation, and application of Bi_2O_2Se, Adv. Funct. Mater. 30 (2020) 2004480.